ELSEVIER

Chemical Engineering Science 60 (2005) 6971–6982

Chemical Engineering Science

www.elsevier.com/locate/ces

# Feasibility study of a reverse flow catalytic membrane reactor with porous membranes for the production of syngas

J. Smit, M. van Sint Annaland*, J.A.M. Kuipers

*Department of Science and Technology, University of Twente, P.O. Box 217, 7500 AE Enschede, The Netherlands*

Received 13 April 2005; received in revised form 18 June 2005; accepted 20 June 2005
Available online 3 August 2005

**Abstract**

In this paper a novel reverse flow catalytic membrane reactor (RFCMR) is proposed for the partial oxidation of $CH_4$ to syngas. The feasibility of the RFCMR concept has been investigated for industrial conditions on basis of a simulation study employing a reactor model, which includes a detailed description of the prevailing heat and mass transfer processes and chemical kinetics of the relevant reactions. It is shown that one of the major cost drivers of a conventional gas-to-liquid process, i.e., the cost associated with the production of pure $O_2$ via cryogenic distillation of air, can be decreased by 25% . Furthermore, a possibly explosive premixed feed is avoided, recuperative heat exchange is fully integrated and very high syngas selectivities are obtained ($>95\%$).


*Keywords:* Reverse flow; Partial oxidation; Membrane reactor; Modelling; Simulation

## 1. Introduction

Natural gas has great potential as feedstock for liquid fuels as an alternative to conventional oil and coal processing. A promising process to convert natural gas to liquid fuels is the so-called gas-to-liquid (GTL) process, in which the partial oxidation of $CH_4$ (POM) is followed by the Fischer–Tropsch (FT) reaction:

$$CH_4 + \tfrac{1}{2}\,O_2 \rightarrow CO + 2H_2,$$

$$nCO + 2nH_2 \rightarrow (CH_2)_n + nH_2O.$$

GTL-processes have been subject of research for over half a century, but have not found widespread application yet because of economic reasons. An important part of the costs of a conventional GTL-plant is related to cryogenic air separation and external heat integration. An alternative air separation and/or heat integration could substantially reduce these costs.

Alternative air separation has recently become possible with the availability of $O_2$ perm-selective perovskite membranes. POM reactors with integrated air separation have already been demonstrated on lab-scale by Balachandran et al. (1995) and also on a pilot plant-scale in the Air Products ITM project. If air separation is integrated inside a POM reactor, very high feed temperatures are required to achieve high syngas yields, because the POM reaction is only slightly exothermic, so that air and $CH_4$ have to be preheated. In view of the very high operating temperatures external heat transfer is very expensive. Therefore, recuperative heat exchange is preferably carried out inside the reactor, which can be achieved with the reverse flow concept (e.g. Matros and Bunimovich, 1996). To combine the POM reaction, the air separation and the recuperative heat exchange into one apparatus, a reverse flow catalytic membrane reactor (RFCMR) was proposed by Smit et al. (2003, 2004).

Also for a conventional, pure $O_2$-based POM reactor, heat integration is costly. In industrial practice (Brejc and Supp, 1989; Aasberg-Petersen et al., 2001) usually $O_2/CH_4$ ratios of 0.6–0.7 are used to partially preheat the feed using the reaction heat (see also Smit et al., 2004). The heat integration

* Corresponding author. Tel.: +31 53 4894478; fax: +31 534 892 882.
*E-mail address:* M.VanSintAnnaland@tnw.utwente.nl (M. van Sint Annaland).

0009-2509/$ - see front matter © 2005 Elsevier Ltd. All rights reserved.
doi:10.1016/j.ces.2005.06.020

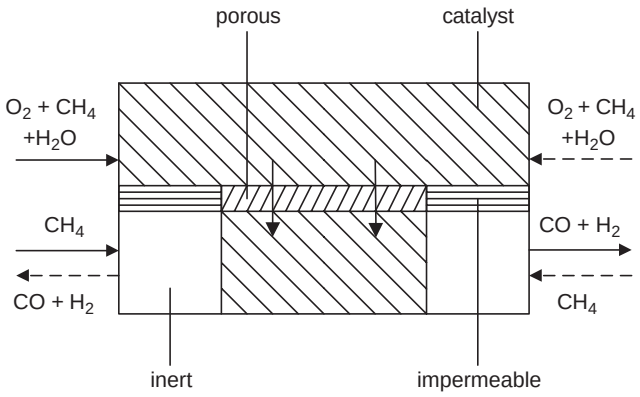


Fig. 1. RFCMR concept with porous membranes.

cost and the $O_2$ consumption can be reduced by integrating the heat exchange inside the POM reactor via the reverse flow concept. A reverse flow reactor for the production of syngas was studied by Blanks et al. (1990), however, based on a premixed $CH_4/O_2$ feed with the accompanying disadvantages of the possible formation of explosive mixtures and low syngas selectivities. The use of a porous membrane or filter in a reverse flow reactor to distributively feed the $O_2$ may overcome these problems. Therefore, a novel reactor is proposed, a RFCMR with porous membranes. This RFCMR basically consists of two compartments (e.g. shell-and-tube configuration). The $O_2$ and syngas compartments are separated by a porous membrane in the centre of the reactor and impermeable walls at the in- and outlets, as schematically represented in Fig. 1. The gas streams are fed co-currently to the compartments and the flow directions are periodically alternated to create the reverse flow behaviour. At the centre, the syngas compartment is filled with catalyst for the POM reaction, while at the in- and outlet of this compartment inert material is positioned for additional heat capacity and to prevent back-reactions. To create the desired trapezoidal temperature profile a small amount of $CH_4$ is added to the $O_2$ feed, which is combusted at the inlet of the $O_2$ compartment (see also Smit et al., 2003). Furthermore, also a small amount of $H_2O$ is added to the $O_2$ feed to maintain the centre of the reactor at more or less isothermal conditions.

In this paper we investigate the possibility to use the RFCMR with porous membranes for the production of syngas by means of a simulation study. Although air separation is not integrated, this novel reactor concept reduces the $O_2$ consumption and heat integration cost of a conventional POM process, making it an interesting alternative if a POM reactor with integrated air separation turns out to be technically and economically unfeasible for operation on industrial scale. Firstly, the reactor model and constitutive relations are discussed. Subsequently, the results of the simulations are presented and the feasibility of the novel reactor concept is assessed.

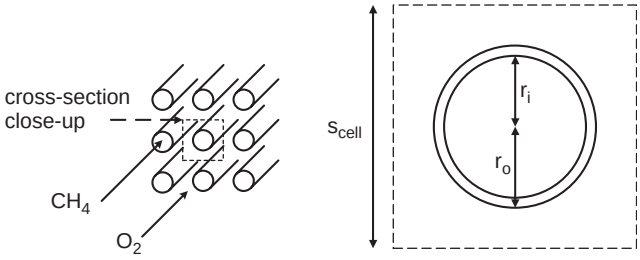


Fig. 2. RFCMR geometry (left) and cross-section close-up (right).

## 2. Reactor model

In this section the reactor configuration and the model assumptions and equations are shortly discussed. Furthermore, the constitutive relations and physical properties are given.

### 2.1. Reactor geometry

To study the feasibility of the RFCMR with porous membranes, a reactor model was developed very similar to that used to study the RFCMR with perovskite membranes (Smit et al., 2003). A shell-and-tube reactor with a square pitch was selected as a possible configuration and is illustrated in Fig. 2. For the reactor model one unit cell is considered, which is assumed to represent the entire tube bank. The geometry of the unit cell is thus determined by its width, the length of the non-permeable walls, the length of the membrane and the inner and outer tube radii. On the tube side, the membrane is filled with POM catalyst, whereas the support tubes are filled with inert $Al_2O_3$ particles. The shell side is filled with a $Pt/Al_2O_3$ combustion catalyst. Furthermore, in our study a ceramic membrane was considered with a macro-porous support and a micro-porous top layer on the inside of the membrane. The permeation rate through the membrane was calculated according to the dusty gas model (Mason and Malinauskas, 1983). However, also other types of distributors could be considered in practical applications such as sintered metal filters or tubes with discrete holes. The only requirements of the porous membrane/filter are that it is resistant to high temperatures and that it has some flow resistance and corresponding pressure drop over the membrane/filter to allow for a good distribution of the gas.

### 2.2. Modelling assumptions and equations

The axial temperature and concentration profiles in the $O_2/H_2O$ and syngas compartments were modelled with a one-dimensional dynamic reactor model (DM) using the following general assumptions:

- Radial temperature and concentration gradients in the compartments were ignored. In this study only the development of the axial temperature profiles was investigated to assess the over-all reactor performance.

Nevertheless, the differences in the tube and shell temperature were accounted for via overall heat transfer coefficients.

- To reduce computational time a homogeneous model (Vortmeyer, 1989; Nieken et al., 1995) was adopted for the description of the thermal behaviour of the reactor.
- The gas phase was assumed to be in pseudostationary-state because of the small gas residence time compared to the switching times, i.e., the accumulation terms in the species conservation equations and switching losses were neglected.

The general model equations of the DM are listed in Table 1. For the boundary conditions the usual Danckwerts-type approach was used. The DM was implemented in an efficient numerical algorithm, which is discussed elsewhere (Smit et al., 2005).

### 2.3. Reaction kinetics and constitutive relations

The POM reactions on the syngas side were described with a heterogeneous model in which the mass transfer from the gas bulk to the catalyst surface was calculated according to the Maxwell–Stefan description (Taylor and Krishna, 1993), which is omitted here because of the lengthy equations. The POM reactions considered are full combustion of $CH_4$, steam and dry reforming of $CH_4$ and the water–gas-shift reaction:

$$\text{I} \quad CH_4 + 2O_2 \rightarrow CO_2 + 2H_2O,$$

$$\text{II} \quad CH_4 + H_2O \rightleftharpoons CO + 3H_2,$$

$$\text{III} \quad CH_4 + CO_2 \rightleftharpoons 2CO + 2H_2,$$

$$\text{IV} \quad CO + H_2O \rightleftharpoons CO_2 + H_2,$$

The POM reaction rates inside the particles were calculated with kinetics taken from Gosiewski et al. (1999) and are given in Table 2. For an accurate description of the effective mass transfer rates at the catalyst surface, principally, the species conservation equations have to be solved inside the particles. Because this requires excessive computational time, the mass transfer rates inside the particles are approximated with a linearisation approach following Gosiewski et al. (1999). In this approach the reaction rates in Table 2 are linearised with respect to the species that has the most significant influence on the reaction rate to obtain an apparent reaction rate constant that is used to calculate the effective reaction rate $R_{\text{eff}}$ via the Thiele modulus:

$$R_{\text{eff}} = R\eta, \tag{15}$$

where the effectiveness factor $\eta$ is calculated with

$$\eta = \frac{3\varphi - \tanh(3\varphi)}{3\varphi^2 \tanh(3\varphi)}, \tag{16}$$

Table 1
Conservations equations used for the dynamic modelling of the RFCMR

Mass conservation equations:

$$\frac{\partial(\rho_g^s v_g^s)}{\partial z} = -\langle M^s\rangle \frac{2\pi r_i}{s_{\text{cell}}^2 - \pi r_o^2} J \tag{1}$$

$$\frac{\partial(\rho_g^t v_g^t)}{\partial z} = \langle M^s\rangle \frac{2}{r_i} J \tag{2}$$

$$\rho_g^s v_g^s \frac{\partial w_{j,g}^s}{\partial z} = \frac{\partial}{\partial z}\left(\rho_g^s D_{\text{ax}}^s \frac{\partial w_{j,g}^s}{\partial z}\right) + r_{j,g}^s \tag{3}$$

$$\rho_g^t v_g^t \frac{\partial w_{j,g}^t}{\partial z} = \frac{\partial}{\partial z}\left(\rho_g^t D_{\text{ax}}^t \frac{\partial w_{j,g}^t}{\partial z}\right) + \frac{6(1-\varepsilon_g^t)}{d_p^t} j_j^t \tag{4}$$

$$+ (1 - w_{j,g}^s)\langle M^s\rangle \frac{2}{r_i} J - j_j^t + r_{j,s}^t = 0 \tag{5}$$

Membrane permeation rate (dusty gas model Mason and Malinauskas, 1983):

$$J = \frac{1}{R_g T^{tw}}\left(K_0 \frac{4}{3}\sqrt{\frac{8R_g T^{tw}}{\pi\langle M^s\rangle}} + B_0 \frac{p_g^s + p_g^t}{2\eta_g^s}\right) \times \frac{(p_g^s - p_g^t)}{(r_i + \delta_m)\ln\left(\frac{r_i + \delta_m}{r_i}\right)} \tag{6}$$

Energy conservation equations:

$$(\varepsilon_g^s \rho_g^s C_{p,g}^s + \rho_{\text{bulk}}^s C_{p,s}^s)\frac{\partial T^s}{\partial t} = -\rho_g^s v_g^s C_{p,g}^s \frac{\partial T^s}{\partial z} + \frac{\partial}{\partial z}\left(\lambda_{\text{eff}}^s \frac{\partial T^s}{\partial z}\right) - \sum_j r_{j,g}^s H_{j,g}^s + \frac{2\pi r_o}{s_{\text{cell}}^2 - \pi r_o^2}\alpha_{s-tw}(T^{tw} - T^s) \tag{7}$$

$$(\varepsilon_g^t \rho_g^t C_{p,g}^t + \rho_{\text{bulk}}^t C_{p,s}^t)\frac{\partial T^t}{\partial t} = -\rho_g^t v_g^t C_{p,g}^t \frac{\partial T^t}{\partial z} + \frac{\partial}{\partial z}\left(\lambda_{\text{eff}}^t \frac{\partial T^t}{\partial z}\right) - \sum_j r_{j,s}^t H_{j,g}^t + \frac{2}{r_i}\alpha_{t-tw}(T^{tw} - T^t) \tag{8}$$

$$\rho_s^{tw} C_{p,s}^{tw} \frac{\partial T^{tw}}{\partial t} = \frac{\partial}{\partial z}\left(\lambda^{tw} \frac{\partial T^{tw}}{\partial z}\right) + \frac{2r_o}{r_o^2 - r_i^2}\alpha_{s-tw}(T^s - T^{tw}) + \frac{2r_i}{r_o^2 - r_i^2}\alpha_{t-tw}(T^t - T^{tw}) \tag{9}$$

and the Thiele modulus $\varphi$ is given by

$$\varphi = \frac{d_p}{6}\sqrt{\frac{k_\eta}{D_{\text{eff}}}}. \tag{17}$$

The linearised reaction rate constants $k_\eta$ were calculated following Gosiewski et al. (1999) and are given in Table 3. However, since $CH_4$ is present in excess for the most

Table 2
POM reaction kinetics (Gosiewski et al., 1999)

$$R_{\mathrm{I}}^{s} = \rho_{\mathrm{bulk}}^{s} k_{\mathrm{I},\infty}^{s} \exp\left(-\frac{E_{a,\mathrm{I}}^{s}}{R_g T^{s}}\right) c_{\mathrm{O_2},s}^{s} c_{\mathrm{CH_4},s}^{s} \tag{10}$$

$$R_{\mathrm{I}}^{t} = \rho_{\mathrm{bulk}}^{t} k_{\mathrm{I},\infty}^{t} \exp\left(-\frac{E_{a,\mathrm{I}}^{t}}{R_g T^{t}}\right) c_{\mathrm{O_2},s}^{t} c_{\mathrm{CH_4},s}^{t} \tag{11}$$

$$R_{\mathrm{II}}^{t} = \rho_{\mathrm{bulk}}^{t} k_{\mathrm{II},\infty}^{t} \exp\left(-\frac{E_{a,\mathrm{II}}^{t}}{R_g T^{t}}\right) c_{\mathrm{H_2O},s}^{t} c_{\mathrm{CH_4},s}^{t} \times \left(1 - \frac{(p_{\mathrm{H_2},s}^{t})^3 p_{\mathrm{CO},s}^{t}}{p_{\mathrm{CH_4},s}^{t} p_{\mathrm{H_2O},s}^{t} (p_g^{\ominus})^2 K_{\mathrm{eq,II}}}\right) \tag{12}$$

$$R_{\mathrm{III}}^{t} = \rho_{\mathrm{bulk}}^{t} k_{\mathrm{III},\infty}^{t} \exp\left(-\frac{E_{a,\mathrm{III}}^{t}}{R_g T^{t}}\right) c_{\mathrm{CO_2},s}^{t} c_{\mathrm{CH_4},s}^{t} \times \left(1 - \frac{(p_{\mathrm{H_2},s}^{t})^2 (p_{\mathrm{CO},s}^{t})^2}{p_{\mathrm{CH_4},s}^{t} p_{\mathrm{CO_2},s}^{t} (p_g^{\ominus})^2 K_{\mathrm{eq,III}}}\right) \tag{13}$$

$$R_{\mathrm{IV}}^{t} = \rho_{\mathrm{bulk}}^{t} k_{\mathrm{IV},\infty}^{t} \exp\left(-\frac{E_{a,\mathrm{IV}}^{t}}{R_g T^{t}}\right) c_{\mathrm{CO},s}^{t} c_{\mathrm{H_2O},s}^{t} \times \left(1 - \frac{p_{\mathrm{H_2},s}^{t} p_{\mathrm{CO_2},s}^{t}}{p_{\mathrm{CO},s}^{t} p_{\mathrm{H_2O},s}^{t} K_{\mathrm{eq,IV}}}\right) \tag{14}$$

Table 3
Linearised POM reaction rate constants

$$k_{\eta,\mathrm{I}}^{s} = \rho_{\mathrm{bulk}}^{s} k_{\mathrm{I},\infty}^{s} \exp\left(-\frac{E_{a,\mathrm{I}}^{s}}{R_g T^{s}}\right) c_{\mathrm{O_2},s}^{s} \tag{18}$$

$$k_{\eta,\mathrm{I}}^{t} = 2\rho_{\mathrm{bulk}}^{t} k_{\mathrm{I},\infty}^{t} \exp\left(-\frac{E_{a,\mathrm{I}}^{t}}{R_g T^{t}}\right) (c_{\mathrm{CH_4},s}^{t} + 0.5 c_{\mathrm{O_2},s}^{t}) \tag{19}$$

$$k_{\eta,\mathrm{II}}^{t} = \rho_{\mathrm{bulk}}^{t} k_{\mathrm{II},\infty}^{t} \exp\left(-\frac{E_{a,\mathrm{II}}^{t}}{R_g T^{t}}\right) c_{\mathrm{CH_4},s}^{t} \tag{20}$$

$$k_{\eta,\mathrm{III}}^{t} = \rho_{\mathrm{bulk}}^{t} k_{\mathrm{III},\infty}^{t} \exp\left(-\frac{E_{a,\mathrm{III}}^{t}}{R_g T^{t}}\right) c_{\mathrm{CH_4},s}^{t} \tag{21}$$

$$c_{\mathrm{CO},s}^{t} > c_{\mathrm{CO},s,eq,\mathrm{IV}}^{t} \Rightarrow k_{\eta,\mathrm{IV}}^{t} = \frac{R_{\mathrm{IV}}^{t}}{c_{\mathrm{CO},s}^{t} - c_{\mathrm{CO},s,\mathrm{eq,IV}}^{t}} \tag{22}$$

$$c_{\mathrm{CO},s}^{t} \leqslant c_{\mathrm{CO},s,eq,\mathrm{IV}}^{t} \Rightarrow k_{\eta,\mathrm{IV}}^{t} = \frac{R_{\mathrm{IV}}^{t}}{c_{\mathrm{CO_2},s}^{t} - c_{\mathrm{CO_2},s,\mathrm{eq,IV}}^{t}} \tag{23}$$

part of the reactor, the linearised reaction rate constants for reactions II and III were linearised with respect to $H_2O$ and $CO_2$, respectively, instead of $CH_4$ (although it was found that this hardly affects the results). The effective diffusivity $D_{\mathrm{eff}}$ in Eq. (17) is calculated via Blanc's law (Reid et al., 1987) and the Knudsen diffusivity:

$$\frac{\varepsilon_s}{\tau D_{\mathrm{eff}}} = \frac{1}{\overline{D_j}} + \frac{1}{D_{\mathrm{KN}}} = \frac{1}{1/\sum_i x_i/D_{i,j}} + \frac{1}{(2/3) r_p \sqrt{8 R_g T/\pi \langle M\rangle}}. \tag{24}$$

The $r_{\mathrm{j}}$ in Eq. (5) are calculated from the $R_{\mathrm{eff}}$ (Eq. (15)):

$$\begin{aligned} r_{\mathrm{CH_4}} &= M_{\mathrm{CH_4}}(-R_{\mathrm{eff,I}} - R_{\mathrm{eff,II}} - R_{\mathrm{eff,III}}),\\ r_{\mathrm{CO}} &= M_{\mathrm{CO}}(R_{\mathrm{eff,II}} + 2R_{\mathrm{eff,III}} - R_{\mathrm{eff,IV}}),\\ r_{\mathrm{CO_2}} &= M_{\mathrm{CO_2}}(R_{\mathrm{eff,I}} - R_{\mathrm{eff,III}} + R_{\mathrm{eff,IV}}),\\ r_{\mathrm{H_2}} &= M_{\mathrm{H_2}}(3R_{\mathrm{eff,II}} + 2R_{\mathrm{eff,III}} + R_{\mathrm{eff,IV}}),\\ r_{\mathrm{H_2O}} &= M_{\mathrm{H_2O}}(2R_{\mathrm{eff,I}} - R_{\mathrm{eff,II}} - R_{\mathrm{eff,IV}}),\\ r_{\mathrm{O_2}} &= M_{\mathrm{O_2}}(-2R_{\mathrm{eff,I}}). \end{aligned} \tag{25}$$

For the combustion of $CH_4$ in the shell compartment the kinetics determined in our lab for a 80 $m^2/g$ 0.5 wt% $Pt/Al_2O_3$ catalyst were used (Smit et al., 2003), which are very similar to that of the combustion kinetics on the tube side, see also Table 4. Because only a small amount of $CH_4$ is combusted in air, the reaction rate can be considered to be pseudo first order with respect to $CH_4$ and also the diffusion coefficient in the calculation of the Thiele modulus can be considered constant, so that the effective reaction rate including internal and external mass transfer can be calculated analytically (Westerterp et al., 1984)

$$R_{j,\mathrm{eff}} = \frac{1}{d_p/(6c_j k_g(1-\varepsilon_g)) + R_j \eta}. \tag{26}$$

In Table 5 the heat and mass transfer coefficients that were used in the simulations are given. The thermal conductivity of the quiescent packed bed was calculated according to Zehner and Schlünder (1970) and the wall-to-bed heat transfer coefficient following Dixon and Creswell (1979), but the lengthy equations are omitted here. The axial pressure drop over the tube and shell compartments was calculated according to the Ergun equation (Ergun, 1952). The physical properties that were used for the simulations were set to typical values encountered in industrial practice and are given in Table 6. Other physical properties were calculated according to Reid et al. (1987) and Daubert and Danner (1985).

## 3. Simulation results

In this section firstly the general reactor dimensions and the reverse flow section of the reactor are discussed. Then simulation results for different POM catalyst diameters and membrane lengths are presented. Subsequently, the axial pressure and temperature profiles are discussed. Finally, the extent of internal and external mass transfer limitations are addressed.

Table 4
Kinetic parameters

| Reaction | $R_I^s$ | $R_I^t$ | $R_{II}^t$ | $R_{III}^t$ | $R_{IV}^t$ |
|---|---|---|---|---|---|
| $k_\infty$ ($m^6$/kg/s/mol) | $14.6 \times 10^3$ | $15.07 \times 10^3$ | $48.82 \times 10^3$ | $6.804 \times 10^3$ | $0.264 \times 10^3$ |
| $E_a$ (kJ/mol) | 98.5 | 100.32 | 114.12 | 142.51 | 38.13 |

Table 5
Heat and mass transfer coefficients

Gas-to-particle heat transfer coefficient (Gunn, 1978):

$$Nu = (7 - 10\varepsilon_g + 5\varepsilon_g^2)(1 + 0.7Re^{0.2}\,Pr^{1/3}) + (1.33 - 2.4\varepsilon_g + 1.2\varepsilon_g^2)Re^{0.7}\,Pr^{1/3} \quad (27)$$

Axial heat dispersion (Gunn and Misbah, 1993):

$$\lambda_{\text{eff}} = \lambda_{\text{bed}} + \frac{Re\,Pr\lambda_g}{Pe_{\text{ax}}} + \frac{Re^2\,Pr^2\lambda_g}{6(1-\varepsilon_g)Nu} \quad (28)$$

$$Pe_{\text{ax}} = \frac{2p}{1-p} \qquad p = 0.17 + 0.33\exp\left(\frac{-24}{Re}\right) \quad (29)$$

Gas-to-particle mass transfer coefficient (Thoenes and Kramers, 1958):

$$k_g = \frac{0.81}{\varepsilon_g}\,v_g\,Re^{-0.5}\,Sc^{-2/3} \quad (30)$$

Axial mass dispersion coefficient (Edwards and Richardson, 1968):

$$\frac{D_{\text{ax}}}{v_g d_p} = \frac{0.73}{Re\,Sc} + \frac{0.5}{1 + 9.7\varepsilon_g\,Re\,Sc} \quad (31)$$

Table 6
Physical properties

| | | | |
|---|---|---|---|
| $B_0$ ($m^2$) | $6.9 \times 10^{-16}$ | $\varepsilon_s^s$, $\varepsilon_s^t$ | 0.6 |
| $K_0$ (m) | $2.24 \times 10^{-9}$ | $\rho_{\text{bulk},Al_2O_3}$ (kg/$m^3$) | 2170 |
| $r_p$ (m) | $9.1 \times 10^{-9}$ | $\rho_{\text{bulk,POM}}$ (kg/$m^3$) | 677 |
| $\delta_m$ (m) | $65 \times 10^{-6}$ | $\rho_{\text{bulk},Pt/Al_2O_3}$ (kg/$m^3$) | 677 |
| $\varepsilon_g^s$, $\varepsilon_g^t$ | 0.4 | $\tau_s^s$, $\tau_s^t$ | 2 |

### 3.1. Reverse flow section

As a starting point, a shell-and-tube configuration with a square pitch was considered as illustrated in Fig. 2. The ratio of the length of the unit cell, $s_{\text{cell}}$, and the tube diameter, $d_t$, is set to 1.25:1. In previous work (Smit et al., 2003) it was already shown that for the RFCMR concept (with integrated air separation) a $CH_4/O_2/H_2O$ molar feed ratio of about 1.13:0.5:0.13 is required to keep the centre of the reactor isothermal and to achieve high syngas yields for typical operating conditions of a pressure of 20 bar and a temperature of about 1500 K on the syngas side. As mentioned earlier, $H_2O$ is co-fed with $O_2$ to the shell compartment, whereas pure $CH_4$ is fed to the tube compartment.

With the design parameters listed above, the axial dimensions can be determined with respect to the in- and outlet sections (i.e., the "reverse flow" part of the reactor). Since the reactor is to operate at elevated pressures and very high temperatures, it is difficult to achieve very high plateau temperatures, if a normal combustion catalyst is used in the in- and outlet section of the shell. This is because of the low ignition temperature of the $CH_4$ combustion (especially if higher pressures are used). For very short switching times and very good heat transfer between the tube and shell compartments, the plateau temperature can be calculated from (Nieken et al., 1995; Smit et al., 2003):

$$\int_{T_{\text{feed}}+\Delta T_{\text{ad}}}^{T_{\text{plateau}}} \frac{M_{CH_4} R^s_{CH_4,\text{eff}}}{w^s_{CH_4,g,\text{in}}}\,dT = \frac{\pi r_i^2 (\rho^s_{g,\text{in}} v^s_{g,\text{in}})^2}{s_{\text{cell}}^2 - \pi r_o^2 + \pi r_i^2} \frac{(-\Delta H_r^s) w^s_{CH_4,g,\text{in}}}{2\langle\lambda_{\text{eff}}\rangle M_{CH_4}}, \quad (32)$$

where $\Delta T_{ad}$ is given by

$$\Delta T_{\text{ad}} = \frac{\pi r_i^2}{s_{\text{cell}}^2 - \pi r_o^2 + \pi r_i^2} \frac{\rho^s_{g,\text{in}} v^s_{g,\text{in}} (\Delta H_r^s) w^s_{CH_4,g,\text{in}}}{\langle\rho_{g,\text{in}} v_{g,\text{in}} C_{p,g}\rangle M_{CH_4}}. \quad (33)$$

The quantities in brackets can be calculated from

$$\langle Y\rangle = \frac{(s_{\text{cell}}^2 - \pi r_o^2)Y^s + \pi r_i^2 Y^t}{s_{\text{cell}}^2 - \pi r_o^2 + \pi r_i^2}. \quad (34)$$

From Eq. (32 it can be calculated that the catalyst activity as listed in Table 4 has to be reduced with a factor of $1 \times 10^5$ to reach a plateau temperature of 1500 K with a reasonable shell $CH_4$ inlet fraction. Since this factor is unrealistic, insertion of inert sections will be considered here.

It is well known that inert sections can be used to increase the plateau temperature dramatically (Nieken et al., 1994; Matros and Bunimovich, 1996). An advantage of using inert sections is that both the plateau temperature as well as the width of the plateau are independent of the reaction kinetics (as long as the reaction is fast enough) so that the reactor can be easily designed and operated. A disadvantage, however, is that the plateau temperature decreases with increasing cycle time (Nieken et al., 1994), so that the cycle time and length of the inert section have to selected simultaneously. If inert sections are used at the in- and outlets of the reactor, the plateau temperature can be estimated from the following relation

$$T_{\text{plateau}} = T_{\text{feed}} + \Delta T_{\text{ad}}\left(1 + \frac{\langle\rho_g v_g\rangle L_{\text{inert}}}{2\langle\lambda_{\text{eff}}\rangle}\right). \quad (35)$$

This relation was taken from literature (Matros and Bunimovich, 1996) but adapted for a (hypothetical) reactor consisting of two separated compartments with co-current flow and with a reaction occurring in one of the compartments. Another important parameter to be considered is the front velocity (Froment, 1990):

$$v_{\text{front}} = \frac{\langle \rho_{g,\text{in}} v_{g,\text{in}} C_{p,g} \rangle}{\langle \rho_{\text{bulk}} C_{p,s} + \varepsilon_g \rho_g C_{p,g} \rangle} \times \left( 1 - \frac{\Delta T_{\text{ad}}}{T_{\text{plateau}} - T_{\text{feed}}} \right). \quad (36)$$

Taking stoichiometric mass fluxes of 1.00 and 0.98 $\text{kg/m}^2/\text{s}$ for the shell and tube compartments (based on an infinitely thin tube), respectively, assuming that the adiabatic temperature rise is relatively small ($\Delta T_{\text{ad}}/(T_{\text{plateau}} - T_{\text{feed}}) \ll 1$) and approximating physical properties at inlet conditions and a temperature of 900 K, a front velocity of about 0.0014 m/s is found. For a reasonable switching time of 300 s, the front would thus travel 0.42 m each cycle and the length of the inert section should be considerably higher to minimise the influence of the cycle time and is therefore set to 2 m. In this case, a $CH_4$ inlet weight fraction of only 0.0006 is required according to Eq. (35) to reach a plateau temperature of 1420 K. As discussed earlier, the required $CH_4$ inlet weight fraction increases with increasing cycle time and has to be found by trial and error with the DM.

### 3.2. Membrane length and POM catalyst diameter

With the axial dimensions for the reverse flow section of the reactor established, the required membrane length and POM catalyst diameter can be determined. These have to be selected simultaneously in such a way that the axial pressure drop over the tube side of the membrane is acceptable, while the particles are sufficiently small to avoid external and internal mass transfer limitations and the residence time is high enough to assure high conversions of reactants via the POM reactions.

To determine the optimal membrane length and POM catalyst particle diameter DM calculations were carried out for several cases. The simulation parameters are listed in Table 7. With respect to the mass fluxes, it was found that it is quite difficult to match the amount of $O_2$ and $CH_4$ with dead-end permeation on the shell side. This implies two boundary conditions for the differential equation governing the shell mass flux (Eq. (1)): a fixed mass flux at the inlet and a zero mass flux at the end. Since this differential equation is only first order, only one boundary condition can be imposed, so that the outlet mass flux has to be controlled with the shell inlet pressure, which requires an artificial by-pass to prevent the shell mass flux from becoming zero leading to numerical instabilities (note that the shell pressure profile and thus the mass fluxes change during a cycle due to the moving temperature profile). Therefore, the tube mass flux was slightly decreased from 1.38 (stoichiometric) to 1.23 $\text{kg/m/s}^2$ in the simulations, so that the shell by-pass was typically 0.1 $\text{kg/m/s}^2$. In practice the shell outlet can simply be closed so that the shell side pressure profile regulates itself.

Table 7
Parameters used in the simulation of the RFCMR

| | | | |
|---|---|---|---|
| $d_{p,\text{Al}_2\text{O}_3}$ (m) | 0.003 | $t_{\text{cycle}}$ (s) | 300 |
| $d_{p,\text{Pt/Al}_2\text{O}_3}$ (m) | 0.003 | $w^t_{g,\text{CH}_4}$ | 1 |
| $d_t$ (m) | 0.025 | $w^s_{g,\text{CH}_4}$ | 0.003 |
| $L_{\text{inert}}$ (m) | 2 | $w^s_{g,\text{H}_2\text{O}}$ | 0.130 |
| $L_{\text{reactor}}$ (m) | 6 | $w^s_{g,\text{O}_2}$ | 0.867 |
| $p^s$, $p^t$ (bar) | ±20 | $\rho^s_g v^s_g$ ($\text{kg/m}^2/\text{s}$) | 1 |
| $r_o - r_i$ (m) | 0.002 | $\rho^s_g v^t_g$ ($\text{kg/m}^2/\text{s}$) | 1.23 |

Table 8
Simulation results for different particle sizes and membrane lengths

| | A | B | C | D | Equilibrium |
|---|---|---|---|---|---|
| $d_{p,\text{POM}}$ (m) | 0.001 | 0.003 | 0.001 | 0.003 | |
| $L_{\text{membrane}}$ (m) | 0.25 | 0.25 | 0.5 | 0.5 | |
| $\langle x^t_{\text{CH}_4,g,\text{out}} \rangle$ | 0.018 | 0.020 | 0.019 | 0.017 | 0.013 |
| $\langle x^t_{\text{CO,g,out}} \rangle$ | 0.312 | 0.310 | 0.312 | 0.311 | 0.314 |
| $\langle x^t_{\text{CO}_2,\text{g,out}} \rangle$ | 0.002 | 0.002 | 0.002 | 0.002 | 0.002 |
| $\langle x^t_{\text{H}_2,\text{g,out}} \rangle$ | 0.655 | 0.652 | 0.656 | 0.653 | 0.659 |
| $\langle x^t_{\text{H}_2\text{O,g,out}} \rangle$ | 0.011 | 0.012 | 0.010 | 0.012 | 0.011 |
| $\langle x^t_{\text{O}_2,\text{g,out}} \rangle$ | 0.001 | 0.004 | 0.001 | 0.002 | 0 |
| $\langle \text{O}_2/\text{CH}_{4,\text{in}} \rangle$ | 0.438 | 0.444 | 0.443 | 0.444 | 0.442 |
| $\langle \text{H}_2\text{O}/\text{CH}_{4,\text{in}} \rangle$ | 0.116 | 0.118 | 0.118 | 0.115 | 0.115 |

In Table 8 the average outlet mole fractions and the accompanying inlet $O_2/CH_4$ and $H_2O/CH_4$ ratios (outlet composition based) are given for the different cases studied. In this table also the equilibrium composition for stoichiometric conditions at 1500 K and 20 bar have been included for $CH_4 : H_2O : O_2 = 1.13 : 0.5 : 0.13$. Note that these ratios are slightly different due to the combustion of a small amount of $CH_4$ in the shell compartment in the simulations. From these results it can be seen that the syngas content ($\langle x_{\text{H}_2,\text{out}} \rangle + \langle x_{\text{CO,out}} \rangle$) is greater than 0.96 for each case and that the CO, $CO_2$, $H_2$ and $H_2O$ fractions are close to the equilibrium values, so very high syngas selectivities can already be obtained for a membrane length of 0.25 m and a POM catalyst particle diameter of 0.003 m. The $CH_4$ fractions are quite dependent on the permeation rate through the membrane, since the permeation rate has to be controlled by the shell side pressure profile, which changes in time as discussed above. Therefore, not too many conclusions can be drawn on the $CH_4$ slip, but it is small anyhow for all these cases. The inlet $O_2/CH_4$ and $H_2O/CH_4$ ratios are typically about 0.44 and 0.12, respectively. Especially the consumption of the expensive $O_2$ is considerably lower (25%)

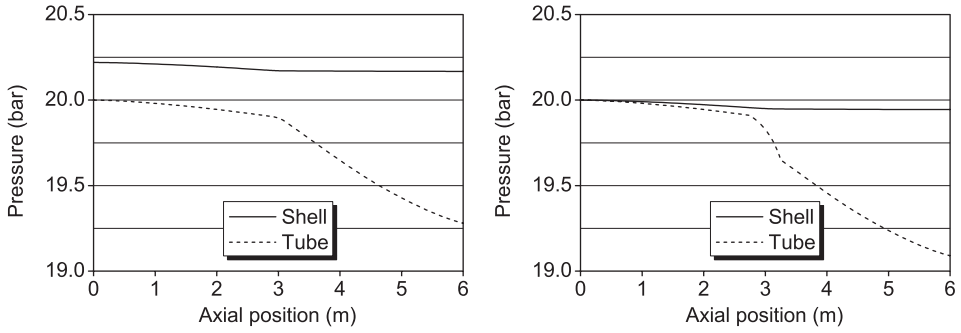


Fig. 3. Axial pressure profiles in the RFCMR at the end of a forward cycle for $d_p = 0.003$ m and $L_{membrane} = 0.25$ m (case B, left) and for $d_p = 0.001$ m and $L_{membrane} = 0.5$ m (case C, right).

compared to industrial practice (Brejc and Supp, 1989; Aasberg-Petersen et al., 2001), where typically $O_2/CH_4 > 0.6$, demonstrating the potential of the RFCMR concept (for a detailed adiabatic thermodynamical analysis of conventional POM processes see Smit et al., 2004). A small amount of $O_2$ is not converted, which is caused by mass transfer limitations as will be discussed later in this section. In the simulations the length of the POM catalyst bed was equal to that of the membrane. Obviously, when the length of the POM catalyst bed is slightly larger than the catalyst bed, all $O_2$ is converted.

### 3.3. Axial pressure and temperature profiles

Typical axial pressure profiles in the RFCMR are given in Fig. 3 for case B and C at the end of a forward cycle. Note that the shell inlet pressures are different for the reasons mentioned in the previous paragraph. The pressure drop on the tube side is the highest for case C, having the longest membrane and the smallest particle diameter, but the difference with case B is small. This is because the pressure drop is mainly due to the outlet part of the tube. Nevertheless, in view of the very steep pressure gradient at the end of the membrane for case C, particle diameters below 0.001 m would lead to unacceptable pressure drops. In practice, the pressure drop that can be allowed and the particle diameter that is required with respect to the external and internal mass transfer rates of the catalyst particle (see next paragraph) will determine the reactor throughput per area.

Typical axial temperature profiles in the RFCMR are given in Fig. 4 for case B. In the centre a reasonably flat temperature profile is established, while close to the inlets the temperature gradients are rather steep. The plateau temperature is not completely flat in the membrane section due to the changing equilibrium compositions along the membrane. At the end of the inert sections small temperature spikes are observed on the shell side, which are due to the combustion of the $CH_4$ that is added to the $O_2$ feed over the $Pt/Al_2O_3$ catalyst. The maximal tube outlet temperature is about 600 K, which is acceptable and also the (radial) difference between the tube and shell temperature as well

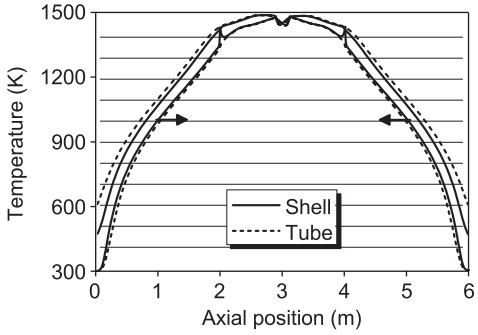


Fig. 4. Axial temperature profiles in the RFCMR at the end of a forward (→) and backward (←) cycle for $d_t = 0.025$ m and $t_{cycle} = 300$ s (case B).

as the (axial) difference between the temperature profiles at the end of a forward and backward cycle is small. The temperature profiles in Fig. 4 were obtained for a tube diameter of 0.025 m and a cycle time of 300 s. Obviously, when larger tube diameters and/or longer cycle times are used, the maximal tube outlet temperature will increase, because of decreased heat transfer from the tube to the shell and the fact that the temperature profile is pushed further into the reactor. In Fig. 5 the axial temperature profiles are shown for case B but now with a cycle time of 600 s (left) and with a tube diameter of 0.05 m (right). In both figures it is observed that the tube outlet temperature is indeed higher, but only about 100 K. When even longer cycle times and/or larger tube diameters are used, the maximal outlet temperature might become a problem, but not for the cases studied here.

Although with the combustion of $CH_4$ in the $O_2$ compartment the reverse flow section and the membrane section are separated, which simplifies both the design and operation due to additional degrees of freedom, it is not essential for the RFCMR concept. This is because the temperature profile is not entirely flat in the membrane section of the RFCMR, but there are temperature peaks at the beginning and end of the membrane section and a temperature dip in the centre. This can be explained by the changing gas composition along the membrane and more specifically the $CO_2$

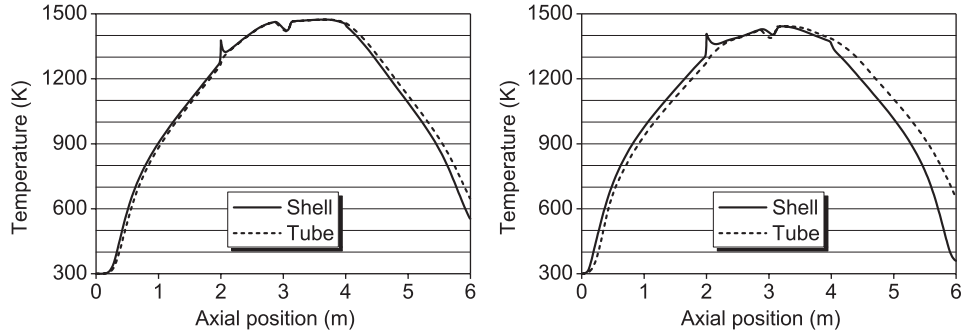


Fig. 5. Axial temperature profiles for $d_t = 0.025$ m and $t_{cycle} = 600$ s (left) and $d_t = 0.05$ m and $t_{cycle} = 300$ s (right) in the RFCMR at the end of a forward cycle (case B).

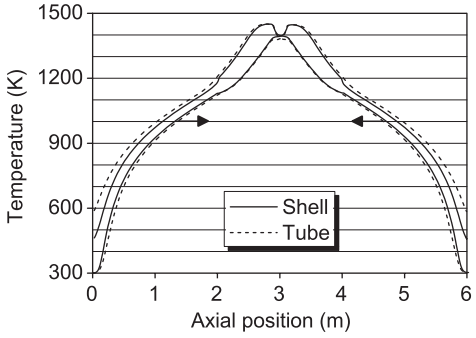


Fig. 6. Axial temperature profiles in the RFCMR at the end of a forward (→) and backward (←) cycle for case B with $w^{S}_{g,CH4} = 0$.

and $H_2O$ mole fractions (see Figs. 7 and 8 in the next paragraph), which indicate that in the beginning and centre of the membrane section primarily CO and $H_2$ are produced and that locally heat is consumed, whereas at the end of the membrane section also significant amounts of $CO_2$ and $H_2O$ are produced and therefore heat is released. This has more or less the same effect with respect to reverse flow behaviour as the combustion of $CH_4$ in the $O_2$ compartment. To illustrate this, a simulation was performed with the operating conditions of case B, but without addition of $CH_4$ to the shell feed. The axial temperature profiles at the end of a cycle are given in Fig. 6. Indeed also without the addition of $CH_4$ to the $O_2$ feed, still a suitable temperature profile can be created and very high syngas selectivities can be achieved. Furthermore, if no $CH_4$ has to be combusted in the shell compartment, also no combustion catalyst is required, which might save on investment costs. However, high syngas selectivities will only be achieved if the temperature is high enough along the membrane and consequently not too long cycle times can be allowed (depending on the membrane length and steepness of the temperature gradients), which limits the operation window. With the combustion of $CH_4$ in the $O_2$ compartment, the reverse flow section and the membrane section are separated, which simplifies both the design and operation. Moreover, the required activity of the catalyst is very low, and hence its prices, since the plateau temperature profile primarily depends on the length of the inert sections in the $O_2$ compartment.

### 3.4. Mass transfer limitations

Typical mole fraction profiles in the RFCMR are given in Figs. 7 and 8 for case A and B, respectively. These figures and in particular the axial profiles of $O_2$ indicate that there are both external and internal mass transfer limitations, which are smaller for smaller particles. The internal mass transfer limitations are confirmed by the low efficiency factors for reactions (I–IV) presented in Fig. 9. However, the influence on the syngas yield is small, especially when considering the fact that gas phase reactions were not accounted for. On the other hand also radial mass transfer limitations were ignored, but this will hardly influence the results, as will be discussed in the next section. When using a longer membrane (see Table 8, case C) or positioning some POM catalyst outside the membrane, equilibrium compositions are easily achieved.

Since the outlet mole fractions are close to equilibrium (Table 8) and the influence of mass transfer limitations is small as discussed above, the question arises whether it is really necessary to use a detailed description of the mass transfer from the gas bulk to the catalyst and inside the catalyst or that simply assuming local thermodynamic equilibrium (e.g. Smit et al., 2003) in the gas bulk is already sufficiently accurate. This reduces the number of equations to be solved considerably and thus the computational effort. Therefore, simulations were carried out for cases A and B in which it was assumed that the gas bulk is locally at equilibrium. In Figs. 10 and 11 the axial profiles of the gas bulk mole fractions are given for cases A and B, with and without mass transfer limitations. For case A, the gas bulk is indeed at local equilibrium due to the small particles and a detailed description of the mass transfer is thus not necessary. For case B, the gas bulk is very close to local equilibrium and the differences are insignificant in view of the assumptions made and the uncertainties in the kinetic rate expressions and with respect to the validity of a number of relations and physical properties used in the model.

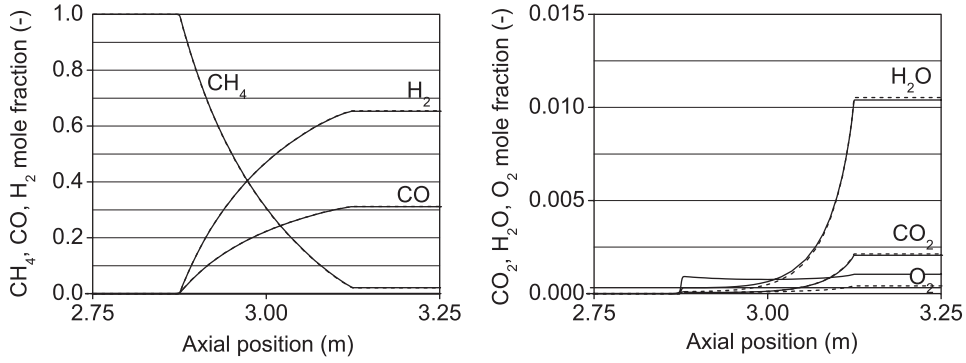


Fig. 7. Axial gas phase (solid line) and catalyst surface (dashed line) mole fraction profiles in the RFCMR at the end of a forward cycle with $d_p = 0.001$ m (case A).

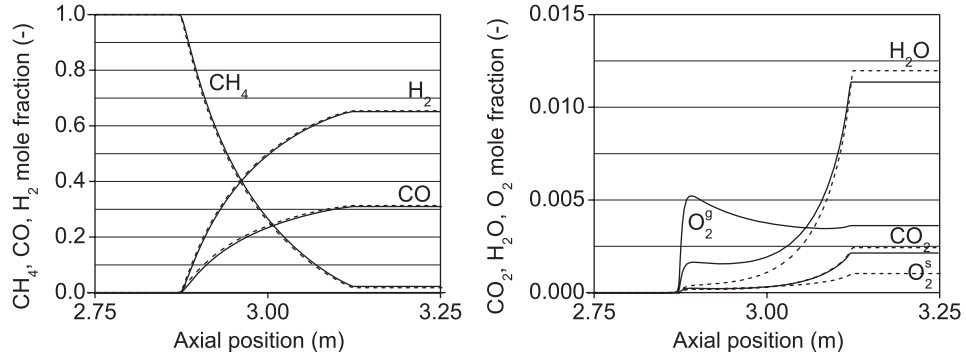


Fig. 8. Axial gas phase (solid line) and catalyst surface (dashed line) mole fraction profiles in the RFCMR at the end of a forward cycle with $d_p = 0.003$ m (case B).

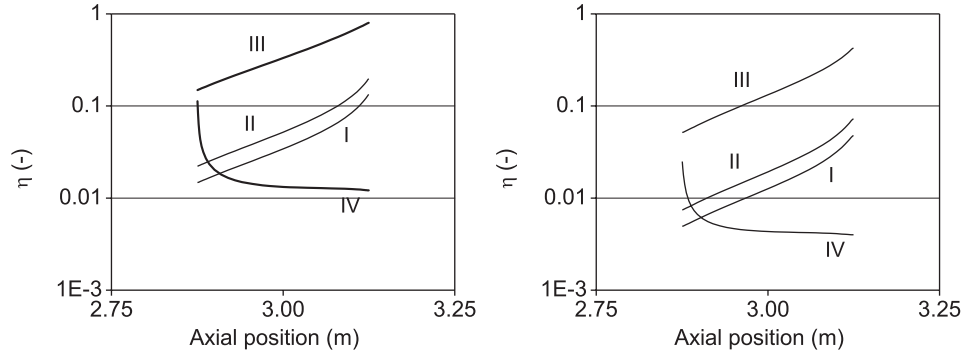


Fig. 9. Axial profiles of the efficiency factors in the RFCMR at the end of a forward cycle with $d_p = 0.001$ m (case A, left) and $d_p = 0.003$ m (case B, right).

## 4. Discussion and conclusions

In this section some assumptions that have been made in the reactor modelling will be discussed. Subsequently, the feasibility of the RFCMR concept with porous membranes will be addressed.

### 4.1. Discussion

In the simulations the gas phase accumulation terms were neglected. In reality, the residence time in the tube compartment is about 13 s for the cases considered in this work. So, for a cycle time of 300 s, this means that about 4% of the tube side output could be considered as switching losses due to unconverted $CH_4$ and combusted syngas. However, for a cycle time of 600 s this already reduces to 2%. In practice the cycle time has to be optimised: it should be long enough to avoid deteriorating the high syngas yields obtained with the RFCMR concept by switching losses, but it should also not be too long, since then a longer reactor would be required.

In this paper a one-dimensional model was considered and radial mass dispersion was not accounted for. To get

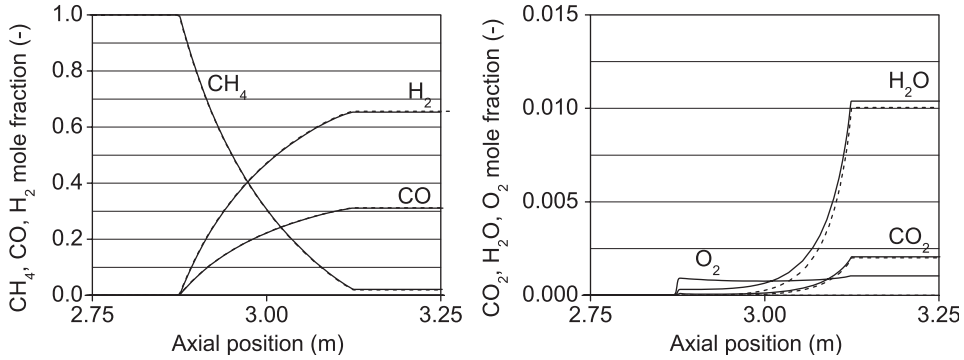


Fig. 10. Axial gas bulk mole fraction profiles in the RFCMR at the end of a forward cycle with (solid line) and without (dashed line) mass transfer limitations (case A).

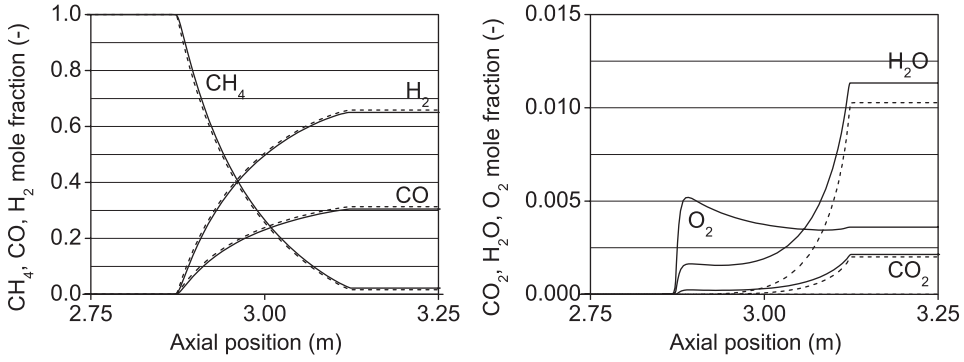


Fig. 11. Axial gas bulk mole fraction profiles in the RFCMR at the end of a forward cycle with (solid line) and without (dashed line) mass transfer limitations (case B).

an idea whether radial mass transfer limitations could affect the presented results, the modified Thiele modulus concept (Kuerten et al., 2004) was used, assuming that the reaction rates are limited by the mass transfer rate from the gas bulk to the catalyst surface. In this case the modified Thiele modulus is given by

$$\varphi = \frac{r_i}{2}\sqrt{\frac{k_g}{D_{\text{rad}}}}, \tag{37}$$

here, the radial mass dispersion is calculated according to Specchia et al. (1980)

$$D_{\text{rad}} = \frac{d_p v_g}{8.65(1 + 19.4(d_p/2r_i)^2)}. \tag{38}$$

From the mass transfer coefficient of Thoenes and Kramers (1958) (Eq. (31)) and using the simulation results of case B in Table 8, it was found that $k_g$ has a typical value of about 0.1 and $\varphi$ a typical value of 0.14. From Eq. (16) it can then be calculated that $\eta = 0.99$, which indicates that there are hardly radial mass transfer limitations and that the one-dimensional results will not be affected. For 0.001 m particles the radial dispersion is smaller and thus the radial mass transfer limitations more pronounced, but still $\eta > 0.95$. To accurately describe the radial mass dispersion a detailed two-dimensional model is required, but it is extremely CPU demanding to solve such a model.

### 4.2. Conclusions

In this paper a novel reverse flow catalytic membrane reactor (RFCMR) with porous membranes for the production of syngas was proposed. A detailed one-dimensional reactor model was developed and with this model simulations were carried out to study the feasibility of the novel reactor concept. The reverse flow part of the reactor was designed with some simple calculations, but the RFCMR was modelled with a detailed description of the prevailing heat and mass transfer processes. Subsequently, simulations were carried out for different particle diameters, membrane lengths, tube diameters and switching times. It was found that very high syngas selectivities (> 95%) can be achieved while fully integrating the recuperative heat exchange. The $O_2$ consumption was reduced with 25% compared to conventional processes and, therefore, the RFCMR concept leads to smaller and less equipment via process intensification, making it a feasible and promising alternative to conventional processes. In the simulations mass transfer limitations were observed, but this hardly affected the syngas compositions. For this feasibility study it was found that it is sufficient to assume that the gas bulk is at local thermodynamic equilibrium.

## Notation

| | |
|---|---|
| $B_0$ | parameter in the dusty gas model, $m^2$ |
| $c_j$ | concentration of species $j$, $mol/m^3$ |
| $C_p$ | heat capacity, J/kg/K |
| $d_p$ | particle diameter, m |
| $d_t$ | tube diameter, m |
| $D_{ax}$ | axial dispersion coefficient, $m^2/s$ |
| $D_{eff}$ | effective diffusivity, $m^2/s$ |
| $D_{i,j}$ | binary diffusion coefficient, $m^2/s$ |
| $\overline{D}_j$ | diffusivity of species $j$ in a mixture, $m^2/s$ |
| $D_{KN}$ | knudsen diffusivity, $m^2/s$ |
| $D_{rad}$ | radial diffusivity, $m^2/s$ |
| $E_a$ | activation energy, J/mol |
| $H_j$ | enthalpy of species $j$, J/mol |
| $\Delta H_r$ | reaction heat, J/mol |
| $j_j$ | mass flux of species $j$, $kg/m^2/s$ |
| $J$ | permeation rate, $mol/m^2/s$ |
| $k_\infty$ | reaction rate constant, 1/s |
| $k_g$ | gas-to-particle mass transfer coefficient, m/s |
| $k_\eta$ | linearised reaction rate constant, 1/s |
| $K_0$ | parameter in the dusty gas model, m |
| $K_{eq}$ | equilibrium constant |
| $L_{inert}$ | length inert section, m |
| $L_{membrane}$ | membrane length, m |
| $L_{reactor}$ | reactor length, m |
| $M_j$ | molar weight of species $j$, kg/mol |
| $\langle M \rangle$ | average molar, kg/mol |
| $Nu$ | dimensionless nusselt number, $\alpha_{g-s} d_p/\lambda_g$ |
| $p$ | parameter in axial heat dispersion coefficient |
| $p$ | pressure, Pa |
| $p_j$ | partial pressure of species $j$, Pa |
| $Pe_{ax}$ | dimensionless Péclet number for axial heat dispersion, $\rho_g v_g d_p C_{p,g}/\lambda_{ax}$ |
| $Pr$ | dimensionless Prandtl number, $C_{p,g}\eta_g/\lambda_g$ |
| $r_i$ | inner tube radius, m |
| $r_j$ | reaction rate of species $j$, $kg/m^3/s$ |
| $r_o$ | outer tube radius, m |
| $r_p$ | pore radius, m |
| $R$ | reaction rate, $mol/m^3/s$ |
| $R_{eff}$ | effective reaction rate, $mol/m^3/s$ |
| $R_g$ | gas constant, 8.314 J/mol/K |
| $Re$ | dimensionless Reynolds number, $\rho_g v_g d_p/\eta_g$ |
| $s_{cell}$ | unit cell length, m |
| $Sc$ | dimensionless Schmidt number, $\eta_g/\rho_g/D$ |
| $t$ | time, s |
| $T$ | temperature, K |
| $T_{feed}$ | feed temperature, K |
| $\Delta T_{ad}$ | adiabatic temperature rise, K |
| $T_{plateau}$ | plateau temperature, K |
| $v$ | superficial velocity, m/s |
| $v_{front}$ | front velocity, m/s |
| $w_j$ | weight fraction of species $j$ |
| $x_j$ | mole fraction of species $j$ |
| $Y$ | dummy variable |
| $z$ | spatial coordinate, m |

*Greek letters*

| | |
|---|---|
| $\alpha_{g-s}$ | gas-to-particle heat transfer coefficient, $J/m^2/K/s$ |
| $\alpha_{t-tw}$ | wall-to-tube heat transfer coefficient, $J/m^2/K/s$ |
| $\alpha_{s-tw}$ | Wall-to-shell heat transfer coefficient, $J/m^2/K/s$ |
| $\delta_m$ | membrane toplayer thickness, m |
| $\varepsilon$ | porosity, dimensionless |
| $\eta$ | effectiveness factor, dimensionless |
| $\eta$ | viscosity, $kg/m^2/s$ |
| $\lambda$ | thermal conductivity, J/m/K/s |
| $\lambda_{ax}$ | axial thermal conductivity, J/m/K/s |
| $\lambda_{bed}$ | thermal conductivity of a quiescent packed bed, J/m/K/s |
| $\lambda_{eff}$ | effective thermal conductivity, J/m/K/s |
| $\rho$ | density, $kg/m^3$ |
| $\rho_{bulk}$ | bulk density of the packed bed, $kg/m^3$ |
| $\tau$ | tortuosity, dimensionless |
| $\varphi$ | Thiele modulus, dimensionless |

*Subscripts*

| | |
|---|---|
| I | $CH_4$ combustion |
| II | $H_2O$ reforming of $CH_4$ |
| III | $CO_2$ reforming of $CH_4$ |
| IV | Water gas shift reaction |
| eq | equilibrium |
| in | inlet |
| $g$ | gas |
| out | outlet |
| $s$ | solid |

*Superscripts*

| | |
|---|---|
| $\ominus$ | at standard pressure |
| $s$ | shell |
| $t$ | tube |
| $tw$ | tubewall |

## Acknowledgements

The authors gratefully acknowledge the financial support of the Dutch Technology Foundation STW, the Energy research Centre of the Netherlands ECN and the Association of Industrial Advisory Council Members of the Dutch Institute for Catalysis Research VIRAN.

## References

Aasberg-Petersen, K., Bak Hansen, J.-H., Christensen, T.S., Dybkjaer, I., Seier Christensen, P., Stub Nielsen, C., Winter Madsen, S.E.L., Rostrup-Nielsen, J.R., 2001. Technologies for large scale gas conversion. Applied Catalysis A-General 221 (1–2), 379–387.

Balachandran, U., Dusek, J.T., Mieville, R.L., Poeppel, R.B., Kleefisch, M.S., Pei, S., Kobylinski, T.P., Udovich, C.A., Bose, A.C., 1995. Dense ceramic membranes for partial oxidation of methane to syngas. Applied Catalysis A-General 133 (1), 19–29.

Blanks, R.F., Wittrig, T.S., Peterson, D.A., 1990. Bidirectional adiabatic synthesis gas generator. Chemical Engineering Science 45 (8), 2407–2413.

Brejc, M., Supp, E., 1989. Non-catalytic partial oxidation and special gasification process for higher-boiling hydrocarbons. In: Elvers, B., Hawkins, S., Ravenscroft, M., Rounsaville, J.F., Shulz, G. (Eds.), Ullmanns Encyclopedia of Industrial Chemistry, fifth ed. vol. A12. VCH Verlagsgesellschaft, Weinheim, Germany, pp. 202–214.

Daubert, T.E., Danner, R.P., 1985. Data Compilation Tables of Properties of Pure Compounds. American Institute of Chemical Engineers, New York.

Dixon, A.G., Creswell, D.L., 1979. Theoretical prediction of effective heat-transfer parameters in packed-beds. A.I.Ch.E. Journal 25 (4), 663–676.

Edwards, M.F., Richardson, J.F., 1968. Gas dispersion in packed beds. Chemical Engineering Science 23, 109–123.

Ergun, S., 1952. Fluid flow through packed columns. Chemical Engineering Progress 48, 89–94.

Froment, G.F., 1990. Reverse flow operation of fixed bed catalytic reactors. In: Matros, Y.S. (Ed.), Unsteady State Processes in Catalysis. VSP, Utrecht, pp. 57–89.

Gosiewski, K., Bartmann, U., Moszcynski, M., Mleczko, L., 1999. Effect of the intraparticle mass transport limitations on temperature profiles and catalytic performance of the reverse-flow reactor for the partial oxidation of methane to synthesis gas. Chemical Engineering Science 54 (20), 4589–4602.

Gunn, D.J., 1978. Transfer of heat or mass to particles in fixed and fluidized beds. International Journal of Heat and Mass Transfer 21 (4), 467–476.

Gunn, D.J., Misbah, M.M.A., 1993. Bayesian estimation of heat transport parameters in fixed beds. International Journal of Heat Mass Transfer 36 (8), 2209–2221.

Kuerten, U., van Sint Annaland, M., Kuipers, J.A.M., 2004. Oxygen distribution in packed bed membrane reactors for partial oxidation systems and its effect on product selectivity. International Journal of Chemical Reaction Engineering 2, A24.

Mason, E.A., Malinauskas, A.P., 1983. Gas Transport in Porous Media: The Dusty Gas Model. Elsevier, Amsterdam.

Matros, Y.S., Bunimovich, G.A., 1996. Reverse-flow operation in fixed bed catalytic reactors. Catalysis Review Science Engineers 38 (1), 1–68.

Nieken, U., Kolios, G., Eigenberger, G., 1994. Fixed-bed reactors with periodic flow reversal: experimental results for catalytic combustion. Catalysis Today 20 (3), 335–350.

Nieken, U., Kolios, G., Eigenberger, G., 1995. Limiting cases and approximate solutions for fixed-bed reactors with periodic flow reversal. A.I.Ch.E. Journal 41 (8), 1915–1925.

Reid, R.C., Prausnitz, J.M., Poling, B.E., 1987. The Properties of Gases and Liquids, fourth ed. McGraw-Hill Inc., New York.

Smit, J., van Sint Annaland, M., Kuipers, J.A.M., 2003. Modelling of a reverse flow catalytic membrane reactor for the partial oxidation of methane. International Journal of Chemical Reaction Engineering 1, A54.

Smit, J., van Sint Annaland, M., Kuipers, J.A.M., 2004. Development of novel reactor concept for the partial oxidation of methane to syngas. Chemical Engineering and Research Design 82 (A2), 245–251.

Smit, J., van Sint Annaland, M., Kuipers, J.A.M., 2005. Grid adaptation with weno schemes for non-uniform grids to solve convection dominated partial differential equations. Chemical Engineering Science 60 (10), 2609–2619.

Specchia, V., Baldi, G., Sicardi, S., 1980. Heat transfer in packed bed reactors with one phase flow. Chemical Engineering and Communication 4, 361–380.

Taylor, R., Krishna, R., 1993. Multicomponent Mass Transfer. Wiley Series in Chemical Engineering, New York.

Thoenes, D., Kramers, H., 1958. Mass transfer from spheres in various regular packings to a flowing fluid. Chemical Engineering Science 8, 271–283.

Vortmeyer, D., 1989. Packed bed thermal dispersion models and consistent sets of coefficients. Chemical Engineering Proceedings 26, 263–268.

Westerterp, K.R., van Swaaij, W.P.M., Beenackers, A.A.C.M., 1984. Chemical Reactor Design and Operation. Wiley, New York.

Zehner, P., Schlünder, E., 1970. Wärmeleitfähigkeit von schüttingen bei mässigentemperaturen. Chem. Ing. Techn. 42 (14), 933–941.